Journal of Molecular Structure 1192 (2019) 264–273

Contents lists available at ScienceDirect

Journal of Molecular Structure

journal homepage: http://www.elsevier.com/locate/molstruc

Transformation of mononuclear dinitrosyl iron complex (DNIC) with thiourea in glutathione aqueous solution

Olesya V. Pokidova [a, *], Nina S. Emel'yanova [a, b], Boris L. Psikha [a], Natalia A. Sanina [a, b], Alexander V. Kulikov [a, b], Alexander I. Kotel'nikov [a, b], Sergey M. Aldoshin [a, b]

[a] Institute of Problems of Chemical Physics of the RAS, Chernogolovka, Moscow Region, 142432, Russian Federation
[b] Lomonosov Moscow State University, Moscow, 119991, Russian Federation

ARTICLE INFO

Article history:
Received 13 March 2019
Received in revised form
2 May 2019
Accepted 3 May 2019
Available online 6 May 2019

Keywords:
Dinitrosyl iron complex
Nitric oxide donors
Glutathione
Thiourea
TDDFT

ABSTRACT

In this work, transformation of DNIC with thiourea ligands, $[Fe(SC(NH_2)_2)_2(NO)_2]Cl \cdot H_2O$ (**I**), in an aqueous buffer solution at neutral pH and in the presence of reduced glutathione (GSH) has been studied. Decomposition of the complex was shown to occur in the buffer solution, with removal of the first thiourea ligand having a higher rate ($k=(3.8 \pm 1.3) \cdot 10^{-4}$ s^{-1}) than the NO group release ($k=(0.7 \pm 0.2) \cdot 10^{-4}$ s^{-1}). This corroborates a quantum-chemical model of **I** decomposition suggested earlier. Using UV–Vis spectrophotometry and EPR spectrometry, the interaction of **I** with GSH in solution was shown to yield a new binuclear tetranitrosyl iron complex (TNIC) with two GS^-- ligands (**II**). Using quantum-chemical modeling, the reaction scheme was suggested, which involves replacement of one thiourea ligand by GS^-, and then dimerization of the forming complexes accompanied by removal of the second thiourea ligand. Theoretical UV–Vis spectra were calculated and interpreted for the initial **I** and for the product of the substitution reaction, **II**.

1. Introduction

Endogenous nitric oxide (NO) is characterized by such biological effect as the ability to form nitrosyl complexes of non-heme iron (NICs), which are found in the cells and tissues of animals, in plants and bacteria [1]. In addition to NO, non-heme iron and competing thiol groups of proteins and low-molecular thiols participate in their formation [2,3]. Over the last years, these complexes have been proved to be a stable form of NO existence in an organism [4,5]: in proteins NICs provide NO stabilization and depositing, while in a low-molecular form they provide NO transfer to the targets.

Synthetic water soluble NICs analogs with functional sulfur-containing ligands are promising prodrugs for the treatment of socially relevant diseases [6,7]. A therapeutic effect of such a hybrid molecule is due to synergism of biologically active thiol and NO activity [8]. It should be noted that NICs stability, including their NO donor activity, is affected considerably not only by the initial structure of the complex but also by components of the biological medium. For instance, deoxyhemoglobin was shown to stabilize TNICs, thus transforming them into more prolonged NO donors [9,10].

The present study investigated the biotransformation of water soluble mononuclear complex **I** (Fig. 1), which spontaneously generates NO into solution. Thiourea and its derivatives are good chelating agents, this being favorable for synthesis of many complexes on their base [11,12]. Such ligands have a wide range of pharmacologic activity, including antituberculosis, antiviral, antibacterial, and antitumor properties [13]. Binuclear complex with N-ethylurea was found to exceed the reference compounds, cisplatin, and satraplatin, with respect to its antitumor potential [14,15]. In addition, based on the structural data and physical-chemical properties of these compounds, we can state that complexes of this type are more efficient NO donors than other NICs [11].

Recently, homogeneous (from the data of small-angle X-ray scattering) water soluble composites of polyvinylpyrrolidone containing these DNICs have been obtained. These polymeric composites keep NO donor activity of initial DNICs and can be used as a targeted drug delivery system [16].

Thus, for these promising DNICs, the study of their biotransformation in solution, and, in particular, their interaction with biological substrates *in vitro* and *in vivo* is the most important step.

* Corresponding author.
E-mail address: pov@icp.ac.ru (O.V. Pokidova).

https://doi.org/10.1016/j.molstruc.2019.05.005
0022-2860/

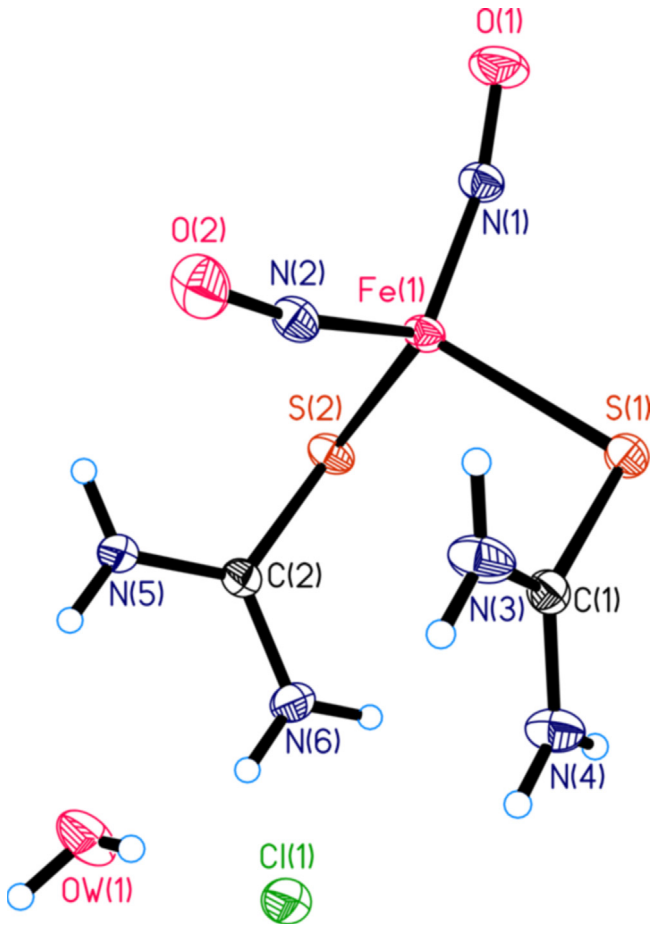

Fig. 1. Molecular structure of cationic mononuclear complex $[Fe(SC(NH_2)_2)_2(NO)_2]Cl \cdot H_2O$ (**I**) (X-ray data published in Refs. [11,12]).

Formerly, decomposition pathways for some NICs with aliphatic and aromatic thioligands have been suggested [17–20]. In aerobic conditions, both NO and nitrosonium ions (NO^+) [17] were shown to release, while in anaerobic conditions only neutral NO groups form [21]. In our works [9,22,23], while studying the decomposition of binuclear TNICs of various classes in anaerobic conditions (NO reaction with deoxyhemoglobin was used for the study), we have also determined that all neutral NO groups release. Decomposition pathway of binuclear TNICs was shown to depend on the redox potential of the initial complexes or the forming intermediates [19,24].

It was found out using the most available non-protein thiol of living organisms, GSH, that in binuclear TNICs of μ-S type with cysteamine and penicillamine ligands GS^- anions substitute for the original thiolate ligands [25,26], while in complexes of μ-N-C-S type no substitution is observed [27]. Based on these data, the assumption was made that antitumor activity of the studied TNICs of μ-S type is due not only to their NO donor activity but also to the ability to bind free GSH in tumor cells. For example, the relationship was discovered between the oxidative stress and oncogenesis, which is based on the glutathionylation of a tumor suppressor p53 [28]. This post-translational modification is typical for many redox-sensitive proteins under oxidative and nitrosative stress conditions [29]. Glutathionylation of p53 supposedly prevents p53 tetramerization, thus suppressing its DNA-binding activity [30]. Thus, TNICs can prevent S-glutathionylation of the tumor suppressor p53, thus restoring its activity and providing an antitumor effect.

Therefore, to design new compounds of the most promising family of NO donors of this class, *viz.*, mononuclear cationic DNICs, it is important to study their ability to substitute GS^- anions for thiourea ligands under conditions similar to physiological ones.

2. Experimental

2.1. Materials and methods

In the work, tris(hydroxymethyl)aminomethane ("Serva", Germany) and L-glutathione in the reduced form ("Aldrich", USA) were used. Water was distilled in a "Bi/Duplex" distiller (Germany).

2.2. Synthesis of **I**

Complex **I** (Fig. 1) was synthesized using the procedure described in Refs. [11,12]. CCDC for **I** – 997479.

2.3. Operation technique in inert gas atmosphere

Operation technique in the inert gas atmosphere was described earlier in Ref. [22].

2.4. Amperometric determination of NO donor activity

The concentration of NO generated by **I** in solutions was measured using a sensor electrode amiNO-700 of "inNO Nitric Oxide Measuring System" (USA). NO concentration was recorded during 500 s (with 0.2 s pace) in the NO donor solution. To calibrate the electrode, a standard aqueous solution of $NaNO_2$ (100 μM) was used, which was added to the mixture containing 20 mg of KI ("Aldrich"), 2 ml of 1 M solution of H_2SO_4 (pure grade, Khimmed), and 18 ml of water [31]. Working solutions of complex **I** were prepared in an aqueous solution using phosphate buffer of pH = 7.0 (HydrionTM, "Aldrich"). All experiments were performed in the temperature-controlled cell at 25°C and intense stirring.

2.5. Complex **I** decomposition at pH 7.0 in Tris-HCl buffer

Anaerobic 0.05 M Tris-HCl buffer pH 7.0 was added to the vessel filled with argon and containing complex **I** sample so that concentration of the complex in solution was $6 \cdot 10^{-4}$ M. Dissolution was performed using magnetic stirrer for 3 min at 23 °C. Then, the aliquot of the solution was taken under an argon flow and inserted in an anaerobic experimental cuvette of 4 ml volume with the optical path length 1 cm, which contained 0.05 M Tris-HCl buffer pH 7.0. The final volume of the complex solution in the experimental cuvette was 3 ml. The reference cuvette contained 3 ml of Tris-HCl buffer pH 7.0.

2.6. Kinetics of **I** interaction with GSH

We used solutions of **I** in 0.05 M Tris-HCl buffer pH 7.0, prepared as described above. 0.3 ml of 10^{-2} M anaerobic GSH solution prepared in 0.1 M Tris-HCl buffer, and 0.1 ml of $6 \cdot 10^{-4}$ M solution of complex **I** were inserted in the anaerobic experimental cuvette containing 2.6 ml of 0.05 M Tris-HCl buffer pH 7.0. The reference cuvette contained 3 ml of Tris-HCl buffer pH 7.0.

2.7. UV–vis absorption spectra

UV–Vis absorption spectra were recorded at 23°C at using an Agilent Cary 60 UV–Vis Spectrophotometer in the range of 200–750 nm at certain time intervals.

2.8. EPR spectra

EPR spectra of complex **I** powder and solutions were registered on a Bruker Elexsys II E 500 EPR spectrometer at room temperature.

The powder was placed in the 5 mm ampoule (inner diameter 4 mm) made of suprasil; aqueous solutions were placed in thin-walled glass ampoules with an inner diameter of 1.0 mm. Below N stands for the ratio of the number of paramagnetic centers determined by EPR to the number of complexes calculated from the sample weight. The number of paramagnetic centers in the samples and g-factor were determined using Xepr program package. To verify the correctness of these procedures, $CuSO_4 \cdot 5H_2O$ sample and diphenyl picrylhydrazyl sample with g-factor 2.0036 were used. The procedure for determination of paramagnetic centers number used in Xepr program package involves double integration of the spectrum and takes into account Q factor of a resonator and spin of paramagnetic centers S. In our case we assumed $S = 1/2$. The accuracy of N value determination is about 15%. For N value determination, the molecular weight of the complex was considered as 321.

2.9. Kinetic modeling

For kinetic simulation, a supposed reaction scheme has been considered, which describes the processes under study. The rate constant values were determined by the least square method based on the numerical solution of the corresponding system of differential equations.

2.10. Quantum-chemical calculations

Quantum-chemical calculations were performed with full geometry optimization of the initial, final, and intermediate complexes using Gaussian 09 program (D version) [32] by means of a local functional BP86 and a basis set 6-311++G**//6-31G* taking into account solvation in an aqueous solution in the frame of polarizable continuum model (PCM). The electronic spectra were calculated by means of the time-dependent density functional theory (TDDFT).

3. Results and discussion

3.1. Decomposition of *I* in buffer aqueous solution

As is well known [1,2,5,33], mononuclear DNICs, unlike binuclear TNICs, are easily identified by a typical signal with $g = 2.03$ in the EPR spectrum. To study complex **I** decomposition, EPR spectra of **I** powder and its aqueous buffer solution were recorded. The shape of the powder EPR spectrum (Fig. 2a) is typical for DNICs powders with axial asymmetry of g-factor with a weak exchange interaction between the complexes [33]. N value is 0.46.

In solution, the anisotropy of g-factor is averaged due to the complex fast rotation; a shape of the EPR spectrum of the complex solution is typical for hyperfine splitting on two equivalent nitrogen atoms with $a_N = 0.21$ mT (Fig. 2 b).

The intensity of the EPR spectrum of the complex solution decreases in time, with invariable line shape (inset, Fig. 2b). The number of paramagnetic centers decreases due to decomposition of complex **I**.

The data of UV–Vis spectrophotometry of **I** decomposition (Fig. 3) confirm the results of EPR spectroscopy: the complex decay and intensity of the optical density in the DNIC absorption maximum at 236 nm ($\varepsilon = 2.54 \cdot 10^4$ $M^{-1}cm^{-1}$) decreases.

In the theoretical UV–Vis spectrum of **I** obtained using TDDFT (Fig. 4), there is also one intense absorption band at 245 nm, which corresponds to the experimental value (236 nm). According to TDDFT calculations, it corresponds to the electron transition from the orbital occupied by the lone pairs of the nitrogen atoms of the thiourea ligands (LP(N)) to the vacant orbital consisting of dz^2 orbitals of Fe and p orbitals of S (inset, Fig. 4).

Thus, this electron transition does not involve the NO groups, and hence, the band at 236 nm in the UV–Vis spectrum only corresponds to the bond between the iron atom and thiourea ligands. Therefore, its decrease in the spectrum is due to the removal of the thiourea ligand, not of NO.

It is known that for the formerly studied cationic DNICs, the band at 390 nm is typical [34,35], which is not observed in the UV–Vis spectrum of complex **I** (Fig. 3). It should be noted that in the theoretical spectrum there is a band at 395 nm, which corresponds to the transition related to the NO ligands, i.e., from the orbital occupied by π electrons of the Fe-N and π^* electrons of NO to the vacant orbital consisting of dxy of Fe and π^* of NO. But its intensity is significantly, by 24 times, less than that of the band at 245 nm.

According to the quantum-chemical calculations performed earlier for complex **I** [36], removal of the thiourea ligand in an aqueous solution is energetically more favorable than that of NO, and the complex decomposition could be accompanied by the thiourea ligand replacement with the water molecule, and by the formation of dimeric intermediates. It should be noted that decomposition of complex **I** is only accompanied by the decrease of intensity of the absorption band at 236 nm in the UV–Vis spectra with time (Fig. 2), while a formation of new bands is not observed, which could be attributed to binuclear TNIC.

For a more thorough study of the mechanism of **I** decomposition, a series of spectrophotometric measurements was performed in 0.05 M Tris-HCl buffer pH 7.0 with various initial concentrations of **I** (Fig. 5).

To elucidate the mechanism and to describe quantitatively the experimental data, the following reaction schemes were considered:

$$I \xrightarrow{k_1} P_1 + L \quad (1)$$

$$P_1 \xrightarrow{k_2} P_2 + L \quad (2)$$

While considering the decomposition process, it is assumed that the change of the absorption maximum intensity at 236 nm is only due to the removal of thiourea ligands (L).

According to the reaction scheme (1)–(2), change of the optical density of the complex solution in time can be presented as:

$$A(t) = (\varepsilon_1[\mathbf{I}] + \varepsilon_2[L] + \varepsilon_3[P_1] + \varepsilon_4[P_2]) \cdot l$$

Values of the extinction coefficients $\varepsilon_1 = 2.54 \cdot 10^4$ $M^{-1}cm^{-1}$ and $\varepsilon_2 = 1.10 \cdot 10^4$ $M^{-1}cm^{-1}$ were determined experimentally, while $\varepsilon_3 = 1.27 \cdot 10^4$ $M^{-1}cm^{-1}$ was estimated from quantum-chemical modeling. ε_4 for $P_2 = 0$. Optical path length $l = 1$ cm.

k_1, k_2 values were determined from minimization of $\Phi(k_1, k_2)$ functional

$$\Phi(k_1, k_2) = \sum_{j=1}^{n} \left(A_{\exp}(t_j) - A_{calc}(t_j)\right)^2$$

which is a sum of deviation squares of the calculated ($A_{calc}(t_j)$) and experimental ($A_{exp}(t_j)$) values of optical density A(t) at certain time moments t_i.

The results of the calculations are presented in Table 1. The obtained values of kinetic parameters satisfactorily describe the experimental data during 5–6 h of the reaction (Fig. 5).

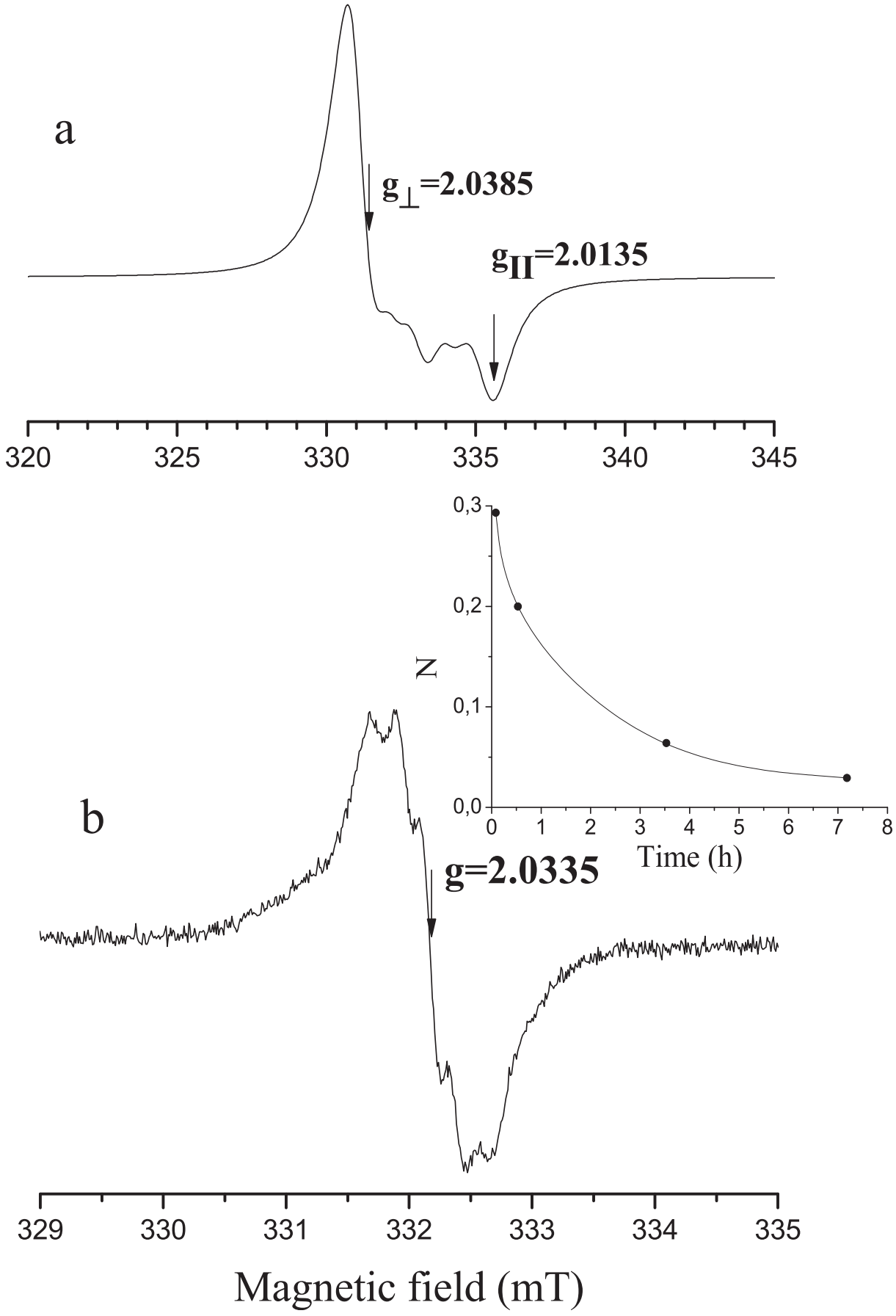

Fig. 2. EPR spectra of the powder (a) and aqueous buffer solution pH 7.0 (b) of complex **I**. The inset shows the time dependence of N after start of dissolution of complex **I**.

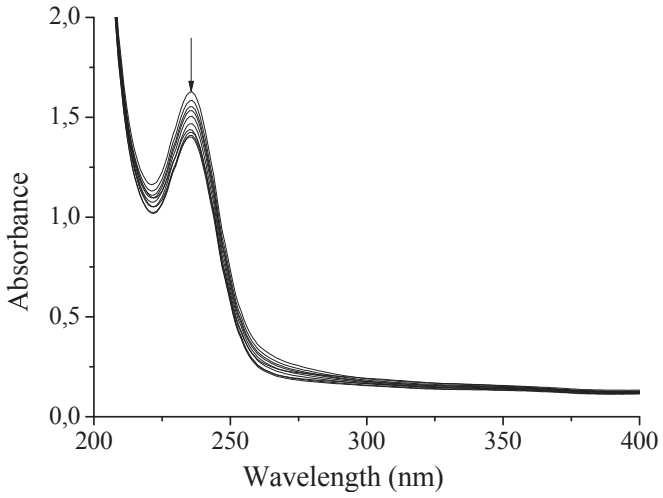

Fig. 3. Kinetics of change of absorption spectra of **I** ($6.65 \cdot 10^{-5}$ M) in time: the spectra were recorded for 6 h. The reaction conditions: 0.05 M Tris-HCl buffer, pH 7.0, T = 23°C.

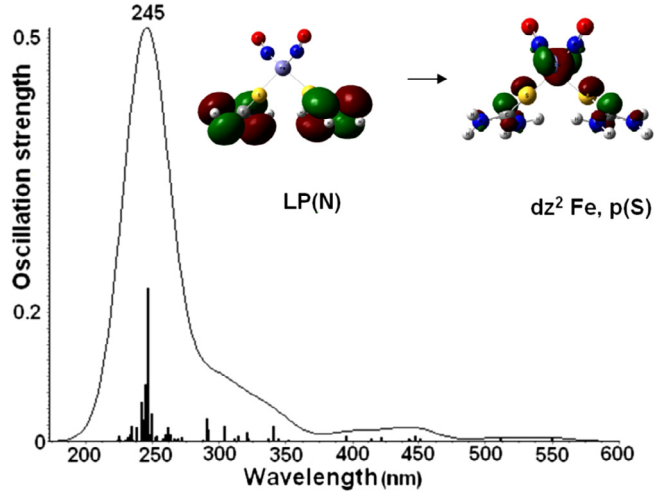

Fig. 4. Theoretical UV–Vis spectrum of **I**. The inset shows the orbitals, which participate in the electron transitions corresponding to the absorption maximum (245 nm) of complex **I**.

To analyze the rate of NO release, a series of experiments with different initial concentrations of **I** was performed using a sensor electrode (Fig. 6).

To describe NO release by complex **I**, the sequence of two reversible reactions was considered:

$$\mathrm{I} \xleftrightarrow[k_{-3}]{k_3} \mathrm{P_3} + \mathrm{NO} \quad (3)$$

$$\mathrm{P_3} \xleftrightarrow[k_{-4}]{k_4} \mathrm{P_4} + \mathrm{NO} \quad (4)$$

The process is supposed to occur as follows. The start of the

Table 1
Rate constants of complex **I** decomposition determined using kinetic modeling.

N№	$[I]_0 \times 10^6$ M	$k_1 \times 10^4$ s^{-1}	$k_2 \times 10^4$ s^{-1}
1	103	3.8	2.1
2	76	5.1	1.8
3	66.5	3.3	0.27
4	64	2.9	1.1

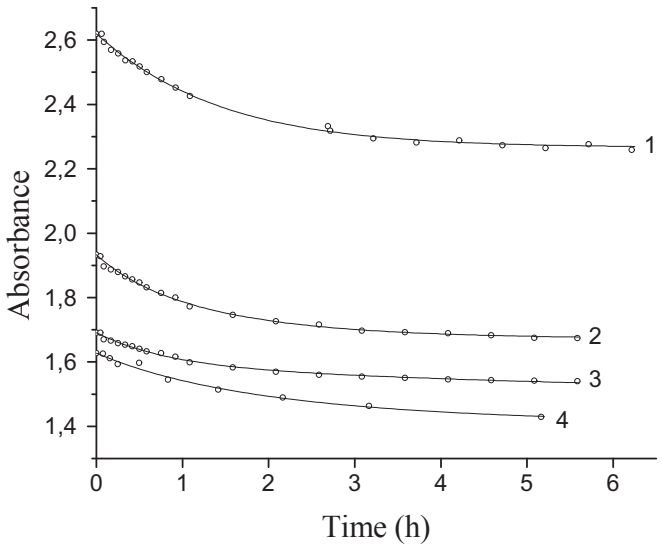

Fig. 5. Kinetics of complex **I** decomposition at 236 nm. Initial concentrations of complex ($[\mathbf{I}]_0$): 10.3×10^{-5} M (1), 7.6×10^{-5} M (2), 6.65×10^{-5} M (3), 6.4×10^{-5} M (4). Circles are the experimental data, solid lines are calculation on the basis of the reaction schemes (1)–(2).

Table 2
Rate constants of complex **I** reactions calculated according to scheme (3)–(4).

N	$[I]_0 \times 10^6$ M	$k_3 \times 10^4$ s^{-1}	$k_{-3} \times 10^{-5}$ M^{-1} s^{-1}	$k_4 \times 10^3$ s^{-1}	$k_{-4} \times 10^{-4}$ M^{-1} s^{-1}
1	11.82	0.915	13.9	5.30	17.4
2	24.88	0.651	14.1	7.59	3.92
3	43.54	0.514	13.1	9.53	2.53

process, according to equation (3), is determined by the constant k_3, then reaction (3) tends to the equilibrium state, this being the reason of the experimental rate decrease. Further, NO release is due to product P_3 decomposition, i.e., is determined by the reaction (4). As shown by the calculations, the considered reaction scheme satisfactorily describes the experimental data.

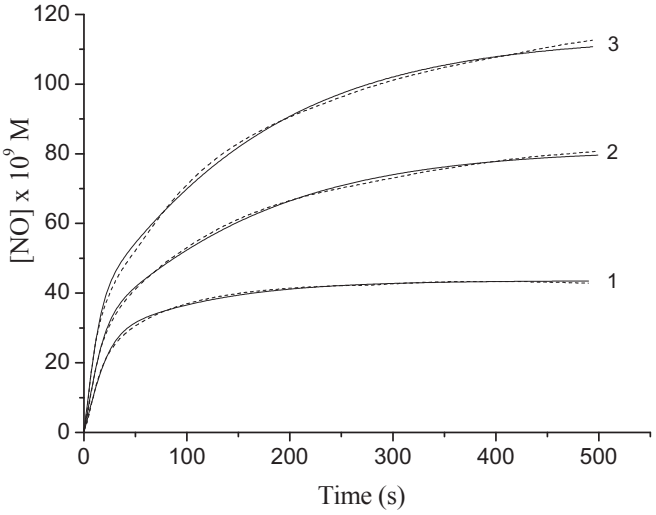

Fig. 6. Kinetic curves of the accumulation of NO in solution (the measurements were carried out by a sensor electrode) in the course of the decomposition of complex **I** in aqueous solution under anaerobic conditions. The complex concentration $[\mathbf{I}]_0$: 11.82 (1), 24.88 (2), 43.54 (3) μM. Dotted lines are the experimental data, solid lines are calculations according to the obtained values of kinetic parameters (Table 2).

The corresponding system of equations is as follows:

$$d[\mathbf{I}]/dt = -k_3[\mathbf{I}] + k_{-3}[P_3][NO]$$

$$d[NO]/dt = k_3[\mathbf{I}] - k_{-3}[P_3][NO] + k_4[P_3] - k_{-4}[P_4][NO]$$

$$d[P_3]/dt = k_3[\mathbf{I}] - k_{-3}[P_3][NO] - k_4[P_3] + k_{-4}[P_4][NO]$$

$$d[P_4]/dt = k_4[P_3] - k_{-4}[P_4][NO]$$

The initial conditions are: $[\mathbf{I}](0) = [\mathbf{I}]_0$; $[NO](0) = [P_3](0) = [P_4](0) = 0$.

Unknown constants k_3, k_{-3}, k_4, k_{-4} were determined in each experiment from the experimental dependence [NO](t) by minimization of functional

$$F(k_3, k_{-3}, k_4, k_{-4}) = \sum_{i=0}^{n} \left([NO]_{exp}(t_i) - [NO]_{calc}(t_i) \right)^2,$$

where $[NO]_{exp}(t_i)$ are experimental [NO] values in the time moments t_i, while $[NO]_{calc}(t_i)$ are the corresponding [NO] values calculated by numerical solution of the equation system. The results are presented in Table 2.

The data of Table 2 quantitatively characterize the ability of the complex to generate NO. The average values of the reaction rate constant are: $k_3 = (0.7 \pm 0.2) \cdot 10^{-4}$ s^{-1}, $k_{-3}=(13.7 \pm 0.4) \cdot 10^5$ $M^{-1}s^{-1}$, $k_4 = (7.5 \pm 2.1) \cdot 10^{-3}$ s^{-1}. A strong dependence of k_4 on the initial concentration of the complex, $[\mathbf{I}]_0$, is apparently due to the fact that not all reactions of product P_4 are taken into account in this mechanism.

The values of the constants (k_1, k_2) and (k_3, k_{-3}, k_4, k_{-4}) were determined from independent experimental data (Figs. 5 and 6). The determination of k_1, k_2 from spectrophotometric measurements did not take into account the reaction of NO release (3)–(4), and when calculating k_3, k_{-3}, k_4, k_{-4} from amperometric measurements, the reaction of the ligand removal (1)–(2) was not taken into account. As a result, the additional consumption of the complex **I** in these reactions was not taken into account. Such an approach is equivalent to the assumption that the NO release does not change the conditions under which the removal of ligand L occurs, and the removal of the ligand does not interfere with the subsequent release of NO. The available experimental data are not enough to confirm or refute this assumption. But it is possible to estimate how the result will change, if we assume that this assumption is not fulfilled. For this, a scheme was considered, including all reactions (1)–(4):

$$d[\mathbf{I}]/dt = -k_1[\mathbf{I}] - k_3[\mathbf{I}] + k_{-3}[P_3][NO]$$

$$d[NO]/dt = k_3[\mathbf{I}] - k_{-3}[P_3][NO] + k_4[P_3] - k_{-4}[P_4][NO]$$

$$d[L]/dt = k_1[\mathbf{I}] + k_2[P_1]$$

$$d[P_1]/dt = k_1[\mathbf{I}] - k_2[P_1]$$

$$d[P_2]/dt = k_2[P_1]$$

$$d[P_3]/dt = k_3[\mathbf{I}] - k_{-3}[P_3][NO] - k_4[P_3] + k_{-4}[P_4][NO]$$

$$d[P_4]/dt = k_4[P_3] - k_{-4}[P_4][NO]$$

The initial conditions are: $[\mathbf{I}](0) = [\mathbf{I}]_0$; concentrations of all other substances are zero.

The constants were determined in an iterative process, using the values of the constants, which were found independently, as the initial approximation. The values of k_1, k_2 were determined from spectrophotometric data (Fig. 5), as described above. As the values of k_3, k_{-3}, k_4, k_{-4} we used the average values of these constants found in the previous step (Table 2). The constants k_3, k_{-3}, k_4, k_{-4} were determined in a similar way from the experimental data of the sensor electrode (Fig. 6); the average values of k_1, k_2 found at the previous iteration were used in the calculation (Table 1).

The final values of the constants are given in Tables 3 and 4 in parentheses. The obtained values of the constants differ little (no more than 2%) from those found earlier in independent experiments. This is explained by the fact that the consumption of the complex **I** in the unaccounted reactions turned out to be small. The removal of ligand L is a slow process that lasts for several hours (Fig. 5), therefore, in 10 min of an experiment with a sensor electrode (Fig. 6) the consumption of complex **I** according to reaction (3) is very small. The effect of the NO release reactions in the experiment on the registration of absorption spectra is even less. Thus, the processes of two independent experiments have no significant effect on each other.

Comparison of the average rate constants for removal of the first thiourea ligand ($k_1=(3.8 \pm 1.3) \cdot 10^{-4}$ s^{-1}) and NO group ($k_3=(0.7 \pm 0.2) \cdot 10^{-4}$ s^{-1}) shows that the ligand removal occurs faster.

Thus, two independent experiments support the data obtained by quantum-chemical modeling [36], *viz*., the ligand removal is the first and the most probable stage of DNIC **I** decomposition.

3.2. *I* interaction with GSH

It has been established [21,22,26] that mono- and binuclear nitrosyl iron complexes in solutions dissociate to release both the thiolate ligand and NO/NO^+. In the presence of GSH, as mentioned above [20,25,26], the GS^- anions substitute for the original thiolate ligands to form TNIC with two GS^- ligands, *viz*, **II**. Decomposition of this compound in anaerobic and aerobic conditions has been studied thoroughly [21,25]. This complex was shown to be the most stable among TNICs with other aliphatic ligands (e.g., cysteine, cysteamine, penicillamine, etc.).

In the case of the mononuclear DNIC **I** under study, the absorption spectrum of the solution immediately changes after the addition of a fourfold excess of GSH, and two absorption maxima appear at 310 and 360 nm (Fig. 7). The shape of the absorption spectrum is similar to that of binuclear TNIC with two GS^--ligands (**II**), and the absorption maxima coincide with literature data [25,34]. The concentration of the resulting binuclear TNIC is two times less than that of the initial complex **I**, thus suggesting complete dimerization of the initial complex. The intensity of the absorption spectra of the obtained TNIC in anaerobic conditions changes inconsiderably in time, this being due to the presence of GSH excess in solution. It should be noted that in aerobic conditions dimerization also occurs immediately after GSH addition.

It should be noted that after adding an excess of GSH to complex **I**, the characteristic for DNIC EPR signal of the reaction product with

Table 3
Rate constants of complex **I** decomposition determined using kinetic modeling.

№	$[I]_0 \times 10^6$ M	$k_1 \times 10^4$ s^{-1}	$k_2 \times 10^4$ s^{-1}
1	103	3.8 (3.7)[a]	2.1 (2.1)
2	76	5.1 (5.0)	1.8 (1.8)
3	66.5	3.3 (3.2)	0.27 (0.27)
4	64	2.9 (2.7)	1.1 (1.2)

[a] The values in parentheses are the values of the constants calculated taking into account reactions (3)–(4).

Table 4
Rate constants of complex **I** reactions calculated according to scheme (3)–(4).

№	$[I]_0 \times 10^6$ M	$k_3 \times 10^4$ s^{-1}	$k_{-3} \times 10^{-5}$ M^{-1} s^{-1}	$k_4 \times 10^3$ s^{-1}	$k_{-4} \times 10^{-4}$ M^{-1} s^{-1}
1	11.82	0.915 (0.933)[a]	13.9 (14.2)	5.30 (5.18)	17.4 (13.4)
2	24.88	0.651 (0.659)	14.1 (14.3)	7.59 (7.79)	3.92 (3.23)
3	43.54	0.514 (0.520)	13.1 (13.4)	9.53 (9.78)	2.53 (2.10)

[a] The values in parentheses are the values of the constants calculated taking into account reactions (1)–(2).

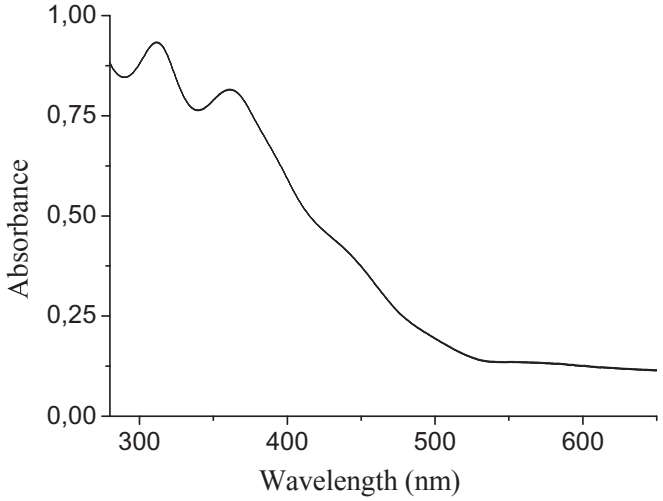

Fig. 7. Absorption spectra of the reaction mixture containing $2 \cdot 10^{-4}$ M **I** and 10^{-3} M GSH. The spectra were recorded for 3 h.

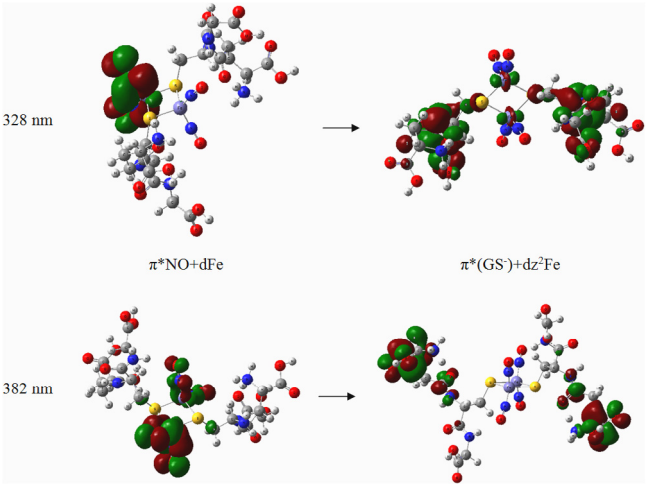

Fig. 9. Electron transitions corresponding to main bands of UV–Vis spectrum for **II**.

g = 2.03 was not detected, this also indicates the formation of diamagnetic TNIC (DNIC dimer). Obviously, upon GSH addition to complex **I** solution, the processes will occur in the system under study, which are similar to those occurring upon **I** decomposition in water solution [36], but involving GSH, with total replacement of the thiourea ligand (UR) by GS^- being energetically more favorable than by water. Scheme 1 shows possible ways of ligands substitution.

As can be seen, replacement of the first UR ligand by GS^- in the initial mononuclear complex is accompanied by the release of 18.44 kcal/mol, while replacement of the second ligand by GS^- is

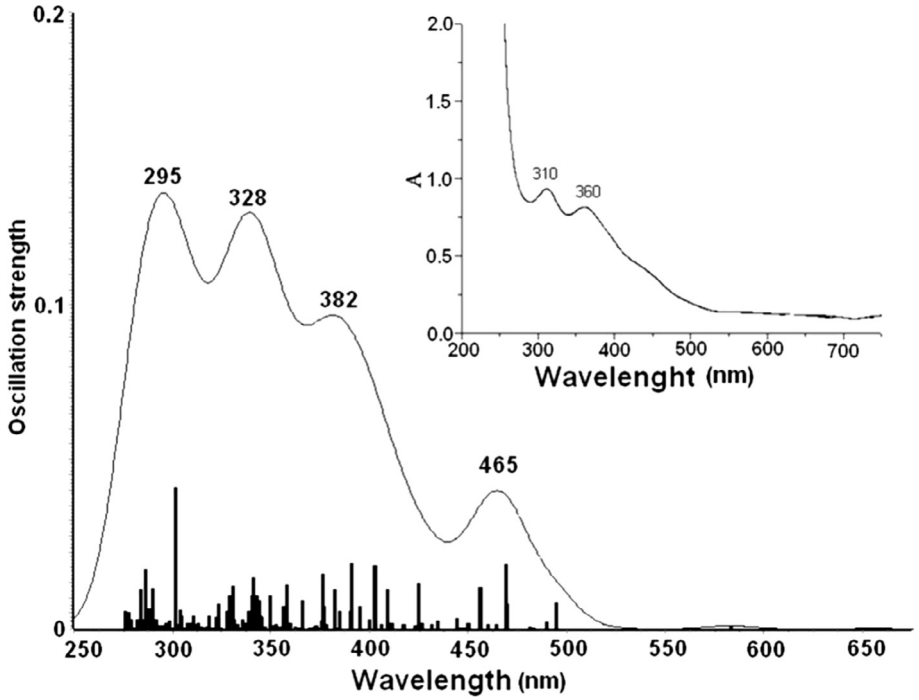

Fig. 8. Simulated UV–Vis spectrum of complex **II.** The inset shows the absorption spectrum of the product of complex **I** and GSH interaction.

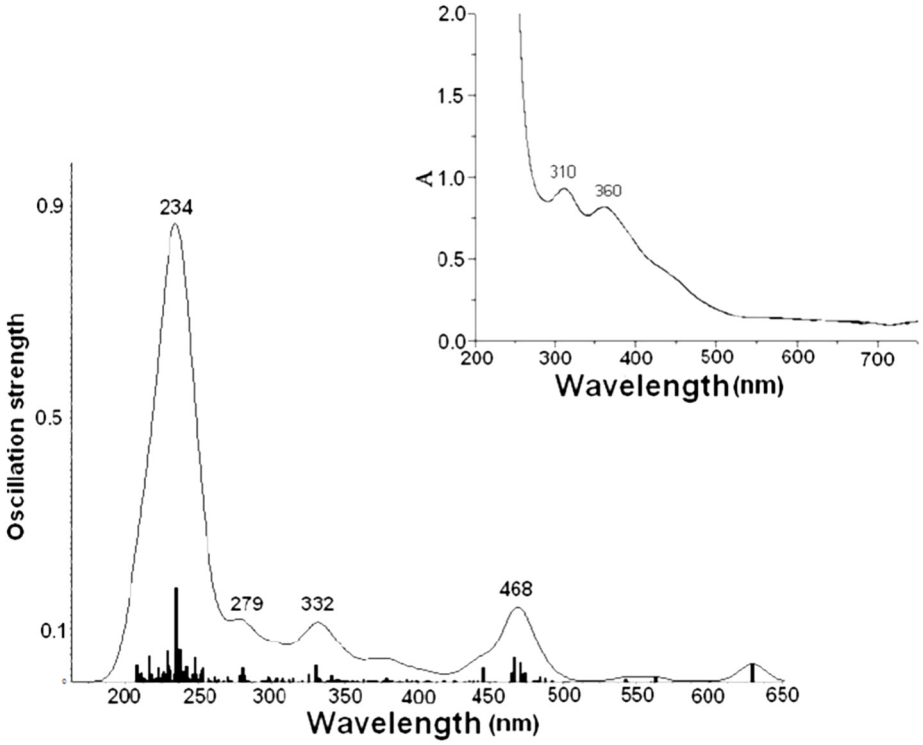

Fig. 10. Simulated UV–Vis spectrum of complex **III.** The inset shows the absorption spectrum of the product of complex **I** and GSH interaction.

thermally neutral.

According to the EPR and absorption spectra, mononuclear DNICs are not final products of the reaction, viz, they undergo dimerization. Product **II** may form from mononuclear DNIC with two GS^- through dimerization with the removal of two GS^- (Scheme 1). The singlet-triple splitting is 33.5 kcal/mol and singlet state lays lower. This is not surprising, because dimer **II** is a Roussin's red salt esters, and they are known to be EPR-silent.

For mononuclear complex $\mathbf{I}^*$, three different dimers may form. Removal of two thiourea ligands yields complex **II**, while removal of one UR and one GS^- results in the formation of binuclear TNIC **III**, however, this reaction being more energetically costly. Dimerization of $\mathbf{I}^*$ to yield **IV**, accompanied by removal of two GS^- ligands, requires a considerable expenditure of energy. Therefore, this reaction is highly unlikely.

On the whole, in the resulting complexes, the Fe-S bond is twice more stable for GS^- than for UR-ligand. Thus, according to quantum-chemical calculations, the interaction of **I** with GSH more likely results in the formation of complex **II** through reaction:

$$2\ [Fe(UR)_2(NO)_2]^+ + 2\ GSH \rightarrow [Fe_2(GS^-)_2(NO)_4]^{2+} + 4UR + H^+$$

As follows from Scheme 1, this total reaction is accompanied by the release of 6.6 kcal/mol. To corroborate that the forming product is actually binuclear TNIC **II**, theoretical spectra of all three probable reaction products were simulated and characterized (Fig. 8–11).

As can be seen, the theoretical spectrum of **II** satisfactorily coincides with the experimental one (Fig. 8). There are 2 bands at 328 and 382 nm, which are compatible with experimental 310 and 360 nm because they correspond to the electron transitions referred to the $Fe(NO)_2$ fragments (Fig. 9). The shift of approximately 20 nm to the long-wave region is not important for this type of calculations [37,38].

The band at 465 nm in the theoretical spectrum appears as a hump in the range of 400–475 nm in the experimental one. It corresponds to the transition from π of Fe-S in the Fe_2S_2 fragment to the π*-orbital of the GS^- - ligand, and is due to the formation of binuclear TNIC.

It should be noted that below 300 nm, free ligands (UR and GSH taken in a fourfold excess) contribute considerably in the absorption spectrum of the reaction mixture (inset, Fig. 8), therefore it is difficult to isolate the calculated intense band at 295 nm, which corresponds to the dFe + LP(S)→ π*(GS^-) transition.

For complex **III**, the situation is different (Fig. 10). As can be seen, the shape of the theoretical spectrum differs essentially from that of the experiment. There are 3 absorption bands at 279, 332, and 468 nm, which cannot be interpreted as a shift because the

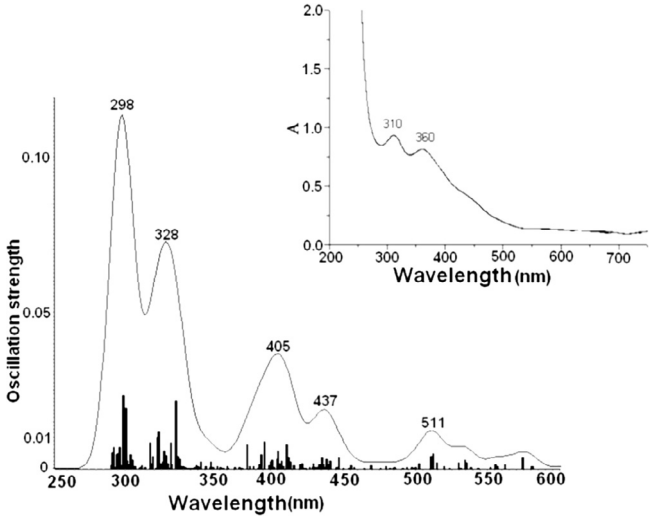

Fig. 11. Simulated UV–Vis spectrum of complex **IV.** The inset shows the absorption spectrum of the product of complex **I** and GSH interaction.

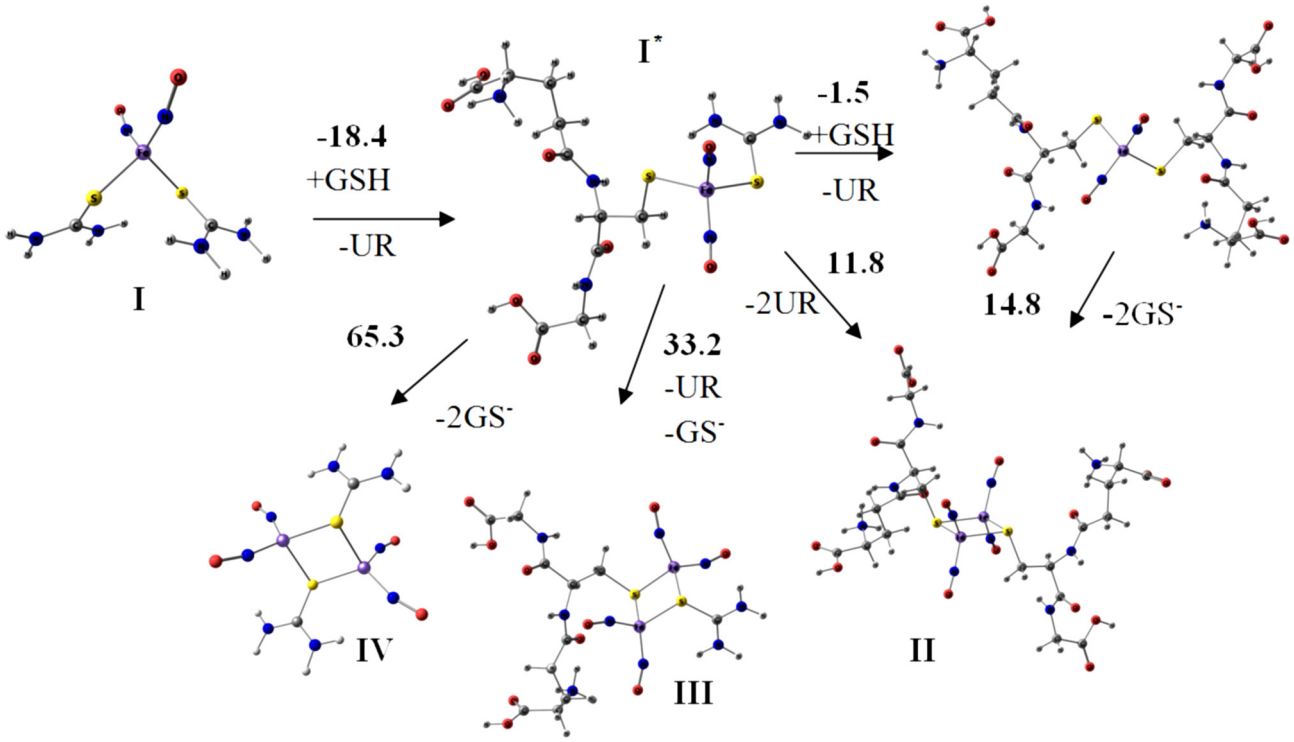

Scheme 1. Scheme of UR replacement by GSH. Values of energy ($\Delta E = E$(products) − E(reagents)) are in kcal/mol.

intensity ratios also differ. Furthermore, in this theoretical spectrum, the bands at 279 nm (transition π*NO + dFe →π*NO + dFe + pS) and 468 nm (transition π*NO + dFe → π*(GS^-)+pN + dz^2Fe) correspond to the $Fe(NO)_2$ groups, as opposed to the experimental spectrum. The band at 332 nm, in contrast to the spectrum of **II**, corresponds to transitions between orbitals involving the π-systems of ligands, p-orbitals of sulfur, and d-orbitals of iron.

Formation of **IV**, as mentioned above, is unlikely because of considerable energetic expenditures. Theoretical UV–Vis spectrum (Fig. 11) is not compatible with the experimental one, similar to the case of dimer **III:** in the experimental spectrum, there is no band at 360 nm.

Thus, as follows from quantum-chemical modeling of theoretical UV–Vis spectra, the experimental spectrum of the product of **I** transformation in an aqueous GSH solution corresponds best of all to the spectrum of binuclear TNIC **II**.

Based on literature data on UV–Vis spectroscopy of complex **II** [25,34], as well as on EPR studies and quantum-chemical calculations of ligands substitution performs in the present work, we can state with certainty that binuclear tetranitrosyl iron complex with two GS^--ligands (**II**) is the reaction product.

4. Conclusions

To further use DNIC as medicines, it is necessary to thoroughly study their probable transformations in solutions in the presence of biologically important cell substrates.

In this work, EPR, UV–Vis spectroscopy, and quantum-chemical and kinetic modeling supplement each other and allow the experiments on DNIC **I** decomposition in an aqueous GSH solution to be interpreted. By means of TDDFT, the band at 236 nm in the absorption spectrum of **I** was shown to correspond to electron transitions, which do not involve the NO groups, but only orbitals of the iron atom and thiourea ligands. Thus, the decrease of the intensity of the DNIC absorption spectrum in time is due to the removal of thiourea ligands. This allowed the kinetic model of DNIC decomposition to be proposed and elementary constants k_1 and k_2 describing this process to be determined.

As follows from the data obtained, the Fe-S bond in the complex under study is weaker than the Fe-N one; therefore, the most likely, removal of thiourea ligands in complexes of this family will occur easier than NO donating. As far as affinity to Fe atom is considerably higher for glutathione ligand than for thiourea one, free GS^- can easily coordinate the iron atoms. In addition, it was found out, that in the neutral medium and with the excess of free GS^-, this process does not stop at the stage of thiourea ligand being replaced by the glutathione one, but the further dimerization of the complex occurs to yield a more stable NO “depot”.

It is important to mention that compounds of this new NO donor class can be used for reducing the quantity of free GSH in tumor cells and for studying molecular-genetic mechanisms of S-glutathionylation *in vivo*.

Acknowledgments

This work was performed in accordance with the state task, state registration No 0089-2019-0014.

References

[1] J.A. McCleverty, Chemistry of nitric oxide relevant to biology, Chem. Rev. 104 (2004) 403–418. https://doi.org/10.1021/cr020623q.
[2] A.R. Butler, I.L. Megson, Non-heme iron nitrosyls in biology, Chem. Rev. 102 (2002) 1155–1166. https://doi.org/10.1021/cr000076d.
[3] A.F. Vanin, P.I. Mordvintcev, S. Hauschildt, A. Mülsch, The relationship between L-arginine-dependent nitric oxide synthesis, nitrite release and dinitrosyl-iron complex formation by activated macrophages, Biochim. Biophys. Acta 1177 (1993) 37–42. https://doi.org/10.1016/0167-4889(93)90154-H.
[4] A.F. Vanin, E. van Faassen, DNIC: physico-chemical properties and their observations in cells and tissues, in: E. van Faassen, A.F. Vanin (Eds.), Radicals for Life: Various Forms of Nitric Oxide, Elsevier Press, 2007, pp. 19–74. https://

doi.org/10.1016/B978-044452236-8/50002-2.
[5] H. Lewandowska, M. Kalinowska, K. Brzóska, K. Wójciuk, G. Wójciuk, M. Kruszewski, Nitrosyl iron complexes—synthesis, structure and biology, Dalton Trans. 40 (2011) 8273–8289. http://doi.org/10.1039/c0dt01244k.
[6] N.Ya Giliano, L.V. Konevega, L.A. Noskin, V.A. Serezhenkov, A.P. Poltoraktov, A.F. Vanin, Dinitrosyl iron complexes with thiol-containing ligands and apoptosis: studies with HeLa cell cultures//, Nitric Oxide 24 (2011) 151–159. http://doi.org/10.1155/2011/878236.
[7] N.A. Sanina, T.N. Rudneva, I.V. Sulimenkov, N.P. Konovalova, T.E. Sashenkova, S.M. Aldoshin, Antitumor activity of iron nitrosyl complexes: new donors of nitrogen monoxide, Ross. Kh. Zh. 53 (2009) 164.
[8] N.A. Sanina, S.M. Aldoshin, Structure and properties of iron nitrosyl complexes with functionalized sulfur-containing ligands, Russ. Chem. Bull. 60 (2011) 1223–1251. https://doi.org/10.1007/s11172-011-0192-x.
[9] L.A. Syrtsova, N.A. Sanina, B.L. Psikha, I.A. Tukhvatullin, N.I. Shkondina, O.V. Pokidova, A.I. Kotelnikov, Interaction of hemoglobin with binuclearcationic tetranitrosyl iron complex with penicillamine. Cations binding sites, Adv. Biol. Chem. 5 (2015) 169–178. https://doi.org/10.4236/abc.2015.53013.
[10] N.A. Sanina, L.A. Syrtsova, E.S. Chudinova, N.I. Shkondina, T.N. Rudneva, A.I. Kotel'nikov, S.M. Aldoshin, Regularities in the stabilization by hemoglobin of binuclear iron complexes [Fe2(μ-N—C—SR)2(NO)4] containing benzimidazolylthiol and benzothiazolylthiol ligands, Russ. Chem. Bull. 58 (2009) 566–571. https://doi.org/10.1007/s11172-009-0057-8.
[11] N.A. Sanina, S.M. Aldoshin, N.Y. Shmatko, D.V. Korchagin, G.V. Shilov, N.S. Ovanesyan, A.V. Kulikov, Mesomeric tautomerism of ligand is a novel pathway for synthesis of cationic dinitrosyl iron complexes: X-ray structure and properties of nitrosyl complex with thiourea, Inorg. Chem. Commun. 49 (2014) 44–47. https://doi.org/10.1016/j.inoche.2014.09.016.
[12] N.A. Sanina, S.M. Aldoshin, N.Y. Shmatko, D.V. Korchagin, G.V. Shilov, E.V. Knyazkina, N.S. Ovanesyan, A.V. Kulikov, Nitrosyl iron complexes with enhanced NO donating ability: synthesis, structure and properties of a new type of salt with the DNIC cations [Fe(SC(NH2)2)2(NO)2]+, New J. Chem. 39 (2015) 1022–1030. https://doi.org/10.1039/C4NJ01693A.
[13] A. Shakeel, A.A. Altaf, A.M. Qureshi, A. Badshah, Thioureas derivatives in drug design and medicinal chemistry: a short review, J. Drug Des. Med. Chem 2 (2016) 10–20. https://doi.org/10.11648/j.jddmc.20160201.12.
[14] N.A. Sanina, N.Y. Shmatko, D.V. Korchagin, G.V. Shilov, A.A. Terent'ev, T.S. Stupina, A.A. Balakina, N.V. Komleva, N.S. Ovanesyan, A.V. Kulikov, S.M. Aldoshin, A new member of the cationic dinitrosyl iron complexes family incorporating N-ethylthiourea is effective against human HeLa and MCF-7 tumor cell lines, J. Coord. Chem. 69 (2016) 812–825. https://doi.org/10.1080/00958972.2016.1142536.
[15] N.A. Sanina, N.Y. Shmatko, T.S. Stupina, A.A. Balakina, A.A. Terent'ev, NO-donor iron nitrosyl complex with n-ethylthiourea ligand exhibits selective toxicity to glioma A172 cells, Molecules 22 (2017) 1426. https://doi.org/10.3390/molecules22091426.
[16] N.Y. Shmatko, N.A. Sanina, D.V. Anokhin, A.A. Piryazev, D.A. Ivanov, A.V. Kulikov, S.M. Aldoshin, Synthesis and properties of polyvinylpyrrolidone films containing iron nitrosyl complexes as nitric oxide (NO) donors with antitumor and antiseptic activities, Russ. Chem. Bull. 64 (2015) 1616–1622. https://doi.org/10.1007/s11172-015-1050-z.
[17] A.F. Vanin, D.S. Burbaev, Electronic and spatial structures of water-soluble dinitrosyl iron complexes with thiol-containing ligands underlying their ability to act as nitric oxide and nitrosonium ion donors, J. Biophy. (2011) 1–14, 2011, https://doi.org/10.1155/2011/878236.
[18] S. Stojanović, D. Stanić, M. Nikolić, M. Spasić, V. Niketić, Iron catalyzed conversion of NO into nitrosonium (NO+) and nitroxyl (HNO/NO−) species, Nitric Oxide 11 (2004) 256–262. https://doi.org/10.1016/j.niox.2004.09.007.
[19] O.V. Pokidova, N.A. Sanina, L.A.L.A. Syrtsova, B.L. Psikha, N.I. Shkondina, A.I. Kotelnikov, S.M. Aldoshin, Two decomposition mechanisms of nitrosyl iron complexes [Fe2(μ-SR)(NO)4], Russ. Chem. Bull. 66 (2017) 432–438. https://doi.org/10.1007/s11172-017-1751-6.
[20] O.V. Pokidova, N.S. Emel'yanova, N.I. Shkondina, A.I. Kotel'nikov, L.A. Syrtsova, N.A. Sanina, S.M. Aldoshin, Features of the decomposition of the neutral nitrosyl iron complexes with aryl-containing thiolate ligands in various solvents. Reaction with glutathione, Russ. Chem. Bull. 66 (2017) 821–827. https://doi.org/10.1007/s11172-017-1813-9.
[21] R.R. Borodulin, L.N. Kubrina, V.D. Mikoyan, A.P. Poltorakov, V.O. Shvydkiy, D.S. Burbaev, V.A. Serezhenkov, E.R. Yakhontova, A.F. Vanin, Dinitrosyl iron complexes with glutathione as NO and NO+ donors, Nitric Oxide 29 (2013) 4–16. https://doi.org/10.1016/j.niox.2012.11.001.
[22] N.A. Sanina, L.A. Syrtsova, N.I. Shkondina, T.N. Rudneva, E.S. Malkova, T.A. Bazanov, A.I. Kotel'nikov, S.M. Aldoshin, Reactions of sulfur-nitrosyl iron complexes of "g=2.03" family with hemoglobin (Hb): kinetics of Hb–NO formation in aqueous solutions, Nitric Oxide 16 (2007) 181–188. https://doi.org/10.1016/j.niox.2006.10.005.
[23] N.A. Sanina, L.A. Syrtsova, B.L. Psikha, N.I. Shkondina, T.N. Rudneva, A.I. Kotel'nikov, S.M. Aldoshin, Ferrocytochrome c and deoxyhemoglobin in the reaction with the iron cysteamine nitrosyl complex {Fe2[S(CH2)2NH3]2(NO)4}SO4·2.5H2O, Russ. Chem. Bull. 59 (2010) 1994–1998. https://doi.org/10.1007/s11172-010-0345-3.
[24] N.A. Sanina, G.V. Shilov, S.M. Aldoshin, A.F. Shestakov, L.A. Syrtsova, N.S. Ovanesyan, E.S. Chudinova, N.L. Shkondina, N.S. Emel'yanova, A.I. Kotel'nikov, Structure of the binuclear tetranitrosyl iron complexes with a pyrimidin-2-yl ligand of the μ2-S type and the pH effect on its NO-donor ability in aqueous solutions, Russ. Chem. Bull. 58 (2009) 572–584. https://doi.org/10.1007/s11172-009-0058-7.
[25] L.A. Syrtsova, N.A. Sanina, E.N. Kabachkov, N.I. Shkondina, A.I. Kotelnikov, S.M. Aldoshin, Exchange of cysteamine, thiol ligand in binuclear cationic tetranitrosyl iron complex, for glutathione, RSC Adv. 4 (2014) 24560–24565. https://doi.org/10.1039/C4RA01766H.
[26] L.A. Syrtsova, N.A. Sanina, K.A. Lyssenko, E.N. Kabachkov, B.L. Psikha, N.I. Shkondina, O.V. Pokidova, A.I. Kotelnikov, S.M. Aldoshin, Reversible dissociation and ligand-glutathione exchange reaction in binuclear cationic tetranitrosyl iron complex with penicillamine, Bioinorgan. Chem. Appl. 2014 (2014) 1–9. https://doi.org/10.1155/2014/641407.
[27] O.V. Pokidova, N.I. Shkondina, T.N. Rudneva, A.I. Kotel'nikov, L.A. Syrtsova, N.A. Sanina, S.M. Aldoshin, Study on the decomposition of iron nitrosyl complex of μ-N-C-S type and its reaction with GSH in aqueous solution, Dokl. Chem. 473 (2017) 49–52. https://doi.org/10.1134/S001250081703003X.
[28] P.M. Chumakov, Versatile functions of p53 protein in multicellular organisms, Biochemist 72 (2007) 1399–1421. https://doi.org/10.1134/S0006297907130019.
[29] P. Klatt, S. Lamas, Regulation of protein function by S-glutathiolation in response to oxidative and nitrosative stress, Eur. J. Biochem. 267 (2000) 4928–4944. https://doi.org/10.1046/j.1432-1327.2000.01601.x.
[30] C.S. Velu, S.K. Niture, C.E. Doneanu, N. Pattabiraman, K.S. Srivenugopal, Human p53 is inhibited by glutathionylation of cysteines present in the proximal DNA-binding domain during oxidative stress, Biochemistry 46 (2007) 7765–7780. https://doi.org/10.1021/bi700425y.
[31] X. Zhang, M.P. Broderick, Amperometric detection of nitric oxide, Mod. Asp. Immunolbiol. 1 (2000) 160–165.
[32] Gaussian 09, Revision D.01 M.J. Frisch, G.W. Trucks, H.B. Schlegel, G.E. Scuseria, M.A. Robb, J.R. Cheeseman, G. Scalmani, V. Barone, B. Mennucci, G.A. Petersson, H. Nakatsuji, M. Caricato, X. Li, H.P. Hratchian, A.F. Izmaylov, J. Bloino, G. Zheng, J.L. Sonnenberg, M. Hada, M. Ehara, K. Toyota, R. Fukuda, J. Hasegawa, M. Ishida, T. Nakajima, Y. Honda, O. Kitao, H. Nakai, T. Vreven, J.A. Montgomery Jr., J.E. Peralta, F. Ogliaro, M. Bearpark, J.J. Heyd, E. Brothers, K.N. Kudin, V.N. Staroverov, T. Keith, R. Kobayashi, J. Normand, K. Raghavachari, A. Rendell, J.C. Burant, S.S. Iyengar, J. Tomasi, M. Cossi, N. Rega, J.M. Millam, M. Klene, J.E. Knox, J.B. Cross, V. Bakken, C. Adamo, J. Jaramillo, R. Gomperts, R.E. Stratmann, O. Yazyev, A.J. Austin, R. Cammi, C. Pomelli, J.W. Ochterski, R.L. Martin, K. Morokuma, V.G. Zakrzewski, G.A. Voth, P. Salvador, J.J. Dannenberg, S. Dapprich, A.D. Daniels, O. Farkas, J.B. Foresman, J.V. Ortiz, J. Cioslowski, D.J. Fox, Gaussian, Inc., Wallingford CT, 2013.
[33] A.F. Vanin, V.A. Serezhenkov, V.D. Mikoyan, M.V. Genkin, The 2.03 signal as an indicator of dinitrosyl–iron complexes with thiol-containing ligands, Nitric Oxide 2 (1998) 224–234. https://doi.org/10.1006/niox.1998.0180.
[34] A.F. Vanin, A.P. Poltorakov, V.D. Mikoyan, L.N. Kubrina, D.S. Burbaev, A.F. Vanin, Polynuclear water-soluble dinitrosyl iron complexes with cysteine or glutathione ligands: electron paramagnetic resonance and optical studies, Nitric Oxide 23 (2010) 136–149. https://doi.org/10.1016/j.niox.2010.05.285.
[35] S. Costanzo, S. Menage, R. Purrello, R.P. Bonomo, M. Fontecave, Re-examination of the formation of dinitrosyl–iron complexes during reaction of S-nitrosothiols with Fe(II), Inorg. Chim. Acta 318 (2001) 1–7. https://doi.org/10.1016/S0020-1693(01)00402-9.
[36] N.S. Emel'yanova, N.Yu Shmatko, N.A. Sanina, S.M. Aldoshin, Quantum chemical modeling of possible reactions of mononuclear iron nitrosyl complex [Fe(SC(NH2)2)2(NO)2]Cl·H2O, Russ. Chem. Bull. 66 (2017) 1842–1846. https://doi.org/10.1007/s11172-017-1955-9.
[37] M. Jaworska, Z. Stasicka, Structure and UV-Vis spectroscopy of the iron-sulfur dinuclear nitrosyl complexes [Fe2S2(NO)4]2− and [Fe2(SR)2(NO)4], New J. Chem. 29 (2005) 604–612. https://doi.org/10.1039/b409519g.
[38] T.T. Lu, C.C. Tsou, H.W. Huang, I.J. Hsu, J.M. Chen, T.S. Kuo, Yu Wang, W.F. Liaw, Anionic Roussin's red esters (RREs) syn-/anti-[Fe(μ-SEt)(NO)2]2−: the critical role of thiolate ligands in regulating the transformation of RREs into dinitrosyl iron complexes and the anionic RREs, Inorg. Chem. 47 (2008) 6040–6050. https://doi.org/10.1021/ic800360m.